PAPER

Check for updates

Phytogenic synthesis of gold–ruthenium (Au–Ru) bimetallic nanoparticles using Aloe vera gel and evaluation of their anticancer potential

Tanjila Begum, [iD] *[a] Sangeeta Agarwal, [iD] [a] Pranab Borah,[b] Akalesh Kumar Verma,[b] Arundhuti Devi[c] and Mausumi Ganguly [iD] [a]

Bimetallic nanoparticles are a key focus in contemporary cancer research because of their efficacy and advantages over conventional monometallic nanoparticles. However, there are very few suitable methods available for their synthesis. Therefore, in the present study, gold–ruthenium (Au–Ru) bimetallic nanoparticles were synthesized using a green, successive-growth approach, with Aloe vera gel acting as a natural reducing and stabilizing agent. The synthesized nanoparticles were characterized using UV-visible spectrophotometry, Fourier Transform Infrared Spectroscopy (FT-IR), High Resolution Transmission Electron Microscopy (HRTEM), Powder X-ray Diffraction (PXRD), Field Emission Scanning Electron Microscopy (FESEM) and Energy Dispersive X-ray spectroscopy (EDX). HRTEM images of Au–Ru NPs at different scales confirm the formation of hexagonal bimetallic Au–Ru NPs of size in the range 19.04–76.19 nm while EDX showed reveals the presence of both the metal. Comparative anticancer evaluation of Au and Au–Ru nanoparticles was carried out in Dalton's lymphoma ascites (DL) cells using the Trypan Blue assay. The IC_{50} value of Au–Ru NPs was 18.34 ± 0.02 μM showing highest potency, while IC_{50} value of AuNPs was 46.7 ± 0.018 μM indicating significantly enhanced anticancer activity. Additionally, bothnanoparticles showed minimal impact (<10%) on non-cancerous PBMC cell lines suggesting it is the least harmful to healthy tissues among the treatments.

1 Introduction

Cancer remains one of the leading causes of global mortality, with poor survival outcomes despite significant progress in diagnostic and therapeutic technologies.[1–3] The Global Cancer Observatory projects nearly 30 million annual cancer-related deaths by 2030.[4] Cisplatin, Cyclophosphamide, 5-fluorouracil are some well-known chemotherapeutic agents used to treat a variety of cancers. However, these medications have several side effects such as toxicity to non-target tissues, nephrotoxicity, gastrointestinal toxicity, cardiovascular, pulmonary, and hematologic toxicity etc.[5] So, new era in cancer research demands new approaches from global research communities to target the cancer cells and thereby to reduce the side effects.

Nanomedicine, an emerging field of research in nanotechnology, has been able to revolutionize several areas including imaging, early disease diagnosis, targeted drug delivery, enhancement of bioavailability of the drug, gene therapy,

phototherapy, chemotherapy etc. As nanomedicines utilizing monometallic nanoparticles have already shown promising results for various cancer therapies, the focus has shifted to bimetallic nanomaterials and exploration of their potential to combat cancer and other malignancies. Nanoparticles in drugs can accumulate at the site of tumors through enhanced permeability and retention (EPR),[6] decreases the side effects of drugs and increases treatment efficiency.[5,7–9]

Bimetallic nanomaterials are of considerable interest due to their synergistic properties of two different metals, which offer their chemical stability and their unique properties compared to their monometallic counterparts. Some common bimetallic combinations such as Ag–Au, Cu–Mn, Pd–Ru, Pt–Ag and Pd–Pt etc. have been reported in several studies against different types of cancer.[10–23]

Among bimetallic nanoparticles studied for anticancer activity, Au–Ru nanoparticles offer novel potential. Gold (Au) nanoparticles are widely explored due to their biocompatibility, ease of functionalization, and surface plasmon resonance, making them useful in drug delivery, photothermal therapy, and imaging.[24,25] Their therapeutic efficiency can be further improved by alloying with ruthenium (Ru), which exhibits stable oxidation states under physiological conditions, participates in redox reactions, and facilitates ligand exchange.[26,27] Au–Ru bimetallic nanoparticles thus combine the advantages of

[a]Department of Chemistry, Cotton University, Guwahati 781001, Assam, India. E-mail: tanjilabegum2016@gmail.com

[b]Department of Zoology, Cell & Biochemical Technology Laboratory, Cotton University, Guwahati 781001, Assam, India

[c]Institute of Advanced Study in Science and Technology (IASST), Guwahati 781033, Assam, India

both metals, providing synergistic effects that enhance anti-cancer activity, stability, and biocompatibility.[28–34] As per author's concern there is no report on anticancer properties of Au–Ru bimetallic nanoparticles till now.

There are several chemical techniques such as chemical reduction, sol–gel processing, electrochemical synthesis, photochemical methods[35] and physical approaches including laser ablation, electrospinning, and ions sputtering are widely used to synthesize nanoparticles with controlled size and morphology. Although these conventional methods are effective, they often require hazardous chemicals, high energy input, and specialized equipment, making them costly and environmentally undesirable.[36] In recent years, biosynthesis has gained significant attention as a greener and more sustainable alternative, utilizing biological systems such as plants, microorganisms, algae, bacteria[37] and enzymes to synthesized nanoparticles under mild conditions.[38] Among these, plant-mediated synthesis is particularly advantageous because plant extracts are readily available, inexpensive, and rich in diverse biomolecules that act simultaneously as reducing, capping, and stabilizing agents.[39,40] This makes plant-based approaches highly suitable for eco-friendly and scalable nanoparticle synthesis.[41–46]

Aloe vera (*Aloe barbadensis* Miller) is a well-known medicinal plant with a wide range of therapeutic properties, including anti-inflammatory, antioxidant, and anticancer effects. It contains various bioactive compounds such as polysaccharides, phenols, and flavonoids, which can act as reducing agents in the synthesis of metal nanoparticles.[47–49] Several works have been reported on green synthesis of nanoparticles using *Aloe vera* gel as reducing and stabilizing agents.[50–53] For instance, *Aloe vera* gel has been employed to synthesize monometallic nanoparticles such as silver, gold, ruthenium, zinc oxide, and copper oxide, where its phytochemicals facilitate rapid reduction of metal ions and contribute to the formation of stable, uniformly dispersed nanoparticles. In addition, *Aloe vera* extracts have been utilized in the fabrication of bimetallic systems, such as Au–Ag, Ag–Cu and Pd–TiO nanoparticles, showing enhanced catalytic and antimicrobial properties owing to synergistic interactions.[54–56] These examples underscore the versatility of *Aloe vera* in green nanotechnology and justify its use as a sustainable, efficient, and eco-friendly reducing agent for bimetallic nanoparticle synthesis in this study. Till now, there is no reports of green synthesis of Au–Ru bimetallic nanopaticles using *Aloe vera* gel.

In this study, we report the first-ever successive-growth–mediated phytogenic synthesis of Au–Ru bimetallic nanoparticles using *Aloe vera* gel, establishing a green, economical, and sustainable alternative to other green and chemical synthesis routes. Furthermore, this study presents first ever comparative evaluation of the anticancer activity of monometallic (Au) and bimetallic (Au–Ru) nanoparticles in Dalton's lymphoma ascites (DL) cells. This study highlights the synergistic effect arising from the combination of the two metals in the bimetallic system. Therefore this study will help the scientific community in further nanomaterial based cancer research.

2 Materials and methods

2.1 Materials

Fresh *Aloe vera* leaves were collected from local area of Jagiroad, Assam, India. Gold(III) chloride trihydrate (HAuCl$_4$·3H$_2$O) and ruthenium(III) chloride (RuCl$_3$·3H$_2$O) were purchased from Loba Chemie. Pvt. Ltd. Gentamicin, streptomycin, penicillin and *cis*-platin were purchased from Merck. All experiments were done using deionized water. Biological samples, including peripheral blood mononuclear cells (PBMC) and Dalton's Lymphoma (DL cell), were donated by Professor Surya Bali Prasad from the Department of Zoology at North Eastern Hill University (NEHU), Shillong, India. These cell lines are currently maintained at the Cell and Biochemical Technology Laboratory, Department of Zoology, Cotton University, Assam, India.

2.2 Preparation of *Aloe vera* extract

Fresh *Aloe vera* leaves were collected and kept vertically for some time to remove the yellow sap material. The leaves were then washed thoroughly with deionized water. The outer green skin was peeled off and the pulp was collected and blended in a mechanical stirrer. The extract was then filtered using Whatmann No. 42 filter paper in order to obtain a clear gel. The gel was stored in a glass bottle in a refrigerator for further use.

2.3 Synthesis of gold nanoparticles (AuNPs)

Gold nanoparticles were synthesized in simple and eco-friendly way using *Aloe vera* gel. Briefly, 50 ml of *Aloe vera* gel was taken in a round bottom flask. 50 ml of 5 mM aqueous solution of HAuCl$_4$·3H$_2$O was added slowly to it and the mixture was stirred for 3 hours at room temperature using a magnetic stirrer. The formation of gold nanoparticles was indicated by a change in the color of the solution from pale yellow to purple (Fig. 1) and confirmed by recording UV-vis spectra.

2.4 Synthesis of gold–ruthenium bimetallic nanoparticles (Au–Ru NP)

In the first step of one pot facile green synthesis of Au–Ru NPs, 40 mL of *Aloe vera* gel was taken in a round bottom flask. 40 ml of 0.5 mM aqueous solution of RuCl$_3$·3H$_2$0 was added to it slowly. The mixed solution was stirred for 3 hours at room temperature. The solution was withdrawn periodically in small volumes and UV-vis spectra were recorded in order to follow the progress of the reaction in the way of the formation of Ru nanoparticles in the *Aloe vera* gel. The change of light brown colour of the solution to dark brown colour visually indicates the formation of Ru nanoparticles which was further confirmed by recording the UV-vis spectra. The solution was kept overnight for the complete synthesis of Ru nanoparticles.

In the second step, 10 ml of *Aloe vera* gel and 10 mL of 5 mM aqueous solution of HAuCl$_4$·3H$_2$O were added to the above solution of Ru nanoparticles. The resulting solution was stirred for another 3 hours. The formation of Au–Ru NPs was visually confirmed by a color change from brownish to dark purple (Fig. 2) and also by recording the UV-vis spectra of the solution.
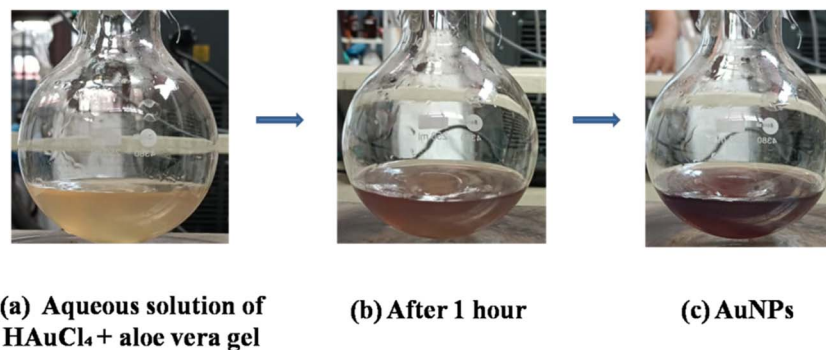
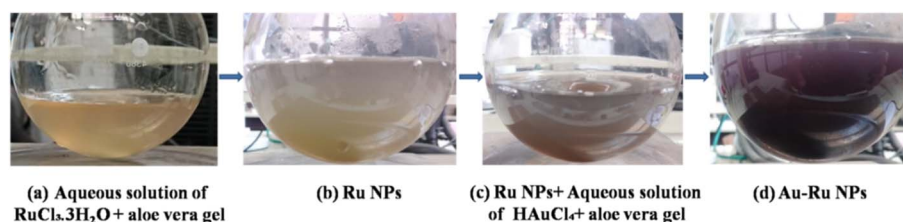**Fig. 1** Green synthesis of AuNPs using *Aloe vera* gel at room temperature.

Fig. 2 Green synthesis of bimetallic Au–Ru NPs using *Aloe vera*.

2.5 Characterisation of AuNPs and Au–Ru NPs

2.5.1 UV-visible spectrophotometry. The UV-vis spectra of AuNP and Au–Ru NP were recorded in the wavelength range of 200–1200 nm to observe the surface plasmon resonance (SPR) peak in UV-2600 spectrophotometer of Shimadzu make.

2.5.2 Fourier transform-infra red spectroscopy (FT-IR) analysis. The FT-IR spectra of the vacuum dried samples of the synthesized AuNPs and Au–Ru NPs were recorded by using KBr pellet method in the wave number range of 500–4000 cm^{-1} using ALPHA BRUKER FT-IR instrument. The sample and anhydrous potassium bromide were mixed in a mortar pestle (in 1 : 100 ratios) and the mixture was placed in between pellet press dies in order to prepare a pellet in a manual hydraulic pellet press machine. The pellet was used for recording the FT-IR spectra of the samples. For comparison, the FT-IR Spectrum of dried *Aloe vera* gel (ALV gel) was also recorded.

2.5.3 FESEM/EDX analysis. The samples (AuNP and Au–RuNP) were dried in a vacuum desiccator and then used for FESEM/EDX analysis. The external morphology and elemental composition of the samples was recorded using Gemini 500 FE-SEM instrument.

2.5.4 High resolution transmission electron microscopic/selected area electron diffraction (HR-TEM/SAED) analysis. The morphology and the size of the nanoparticles were determined using HR-TEM images recorded at different scales (200 nm, 100 nm, 50 nm, 20 nm, 10 nm, 5 nm and 2 nm) in TEM instrument (JEOL JEM-2100) operating at an accelerating voltage of 200 kV. For recording HRTEM images, a drop of the suspension of the sample in isopropanol was placed on a Cu grid and dried in vacuum oven. The SAED (Selected Area Electron Diffraction) pattern was also recorded at 51 nm scale.

2.5.5 Powder XRD analysis. The vacuum dried AuNPs and Au–Ru NPs were used for powder XRD analysis. The powder XRD pattern was recorded in the 2θ region (3° to 80°) with step size 0.02° min^{-1} using Cu-Kα radiation of wavelength 1.5406 Å, nickel monochromator filtering wave tube having 40 kV voltage and 30 mA tube current (Bruker D8 Advance).

2.5.6 Zeta potential. For zeta potential measurement, the samples (AuNP, Au–Ru NP) were added to de-ionised water and sonicated for two hours and the resulting dispersion was used for analysis using a zetasizer, ZS90 instrument (model no. ZEN3690).

2.6 Cytotoxicity assay

2.6.1 Cell line and drug preparation. Cancer research relies on robust pre-clinical models to evaluate potential therapeutic agents. Dalton's lymphoma is particularly useful, as documented by Klein (1951).[57] This aggressive T-cell lymphoma provides a valuable model for assessing various drug candidates, yielding reliable biological endpoints like predictable survival times and observable tumor growth patterns.[58] To establish a safety profile, peripheral blood mononuclear cells (PBMCs) were included in the study. PBMCs, a non-cancerous cell line is useful for evaluating the potential toxicity of novel drug molecules, as described by Pourahmad and Salimi (2015).[59] In this study, cells were cultured in RPMI media with 10% Fetal Bovine Serum (FBS), 100 μg mL^{-1} streptomycin, 100 U per mL penicillin, and maintained at 37 °C with 5% CO$_2$. Different concentrations (0.01, 0.1, 0.5, 1, 5 and 10 μM) of cisplatin (reference drug), ALV gel, Au–Ru NP and AuNP were prepared in conditioned culture media (pH 7.4, at 37 °C with 5% CO$_2$).To determine the IC$_{50}$ values of cisplatin (the reference drug), ALV gel, Au–Ru NP, and AuNP, DL cells were treated with varying concentrations of 5, 10, 20, 40, 60, 80 and 100 μM for 48 hours.

2.6.2 Trypan blue cytotoxicity assay. The trypan blue exclusion assay serves as a cornerstone technique in cancer research for assessing cell viability and quantifying the cytotoxic effects of various treatment regimens.[60] This well-established assay relies on the selective permeability of trypan blue dye. Live cells, possessing intact cell membranes, effectively exclude the dye. Conversely, compromised membranes in non-viable (dead) cells allow trypan blue to penetrate and stain the cytoplasm, resulting in a distinct blue coloration.[61] In the present study, we employed the trypan blue exclusion experiment to evaluate the antiproliferative and cytotoxic potential of the ALV gel, Au–Ru NP, and AuNP on both cancerous (DL) and normal (PBMC) cell lines after 48 h of *in vitro* treatment. This dual evaluation allows us to not only assess the efficacy of the compounds against cancer cells but also to determine their potential toxicity towards healthy cells.[62] Various concentrations (0.01–10 μM) of compounds were used to study potential cytotoxicity on 96 cell culture plates (Thermo Scientific, Cat. No: 265301). After 48 h of *in vitro* treatment in suitable culture media, cells were stained (3 min) with trypan blue dye (0.4%). Finally, 1000 cells were counted considering multiple view fields from each experimental group ($n = 3$) to assess the percentage of cytotoxicity over control. Subsequently, the IC_{50} value was determined using a non-linear regression curve-fitting model, as described by the following function:

$$y = A_1 + (A_2 - A_1)/(1 + 10^{(\log x_0 - x) \times p})$$ (1)

where, A_1 = bottom asymptote, A_2 = top asymptote, $\log x_0$ = center and p = hill slope.

2.6.3 Statistical analysis. The results were expressed as mean ± S.D. (standard deviation) of three independent experiments. Data were analyzed for normality test using Shapiro–Wilk's W test and was further analyzed for one-way ANOVA. All the differences were considered significant at the 95% confident level ($P < 0.05$).

3 Result and discussion

3.1 UV-visible spectrophotometric analysis

The UV-vis spectrum of aqueous auric acid stock solution shows a charge transfer band at 274 nm and a d–d transition band at 367 nm. The formation of the Au nanoparticles was confirmed by the visual change of colour as well as by the disappearance of peaks due to Au^{3+} ions and the appearance of the characteristic surface plasmon resonance (SPR) peak at 547 nm as shown in Fig. 3. The literature survey also reports the SPR peak of gold nanoparticle in the range 536 nm to 546 nm[63–65].

In the first step of the synthesis of bimetallic Au–Ru nanoparticles, the Ru nanoparticles were first synthesized using *Aloe vera* gel at room temperature. The UV-vis spectrum of $RuCl_3 \cdot 3H_2O$ exhibits d–d transition bands at 311 nm and 497 nm respectively as shown in Fig. 4. Disappearance of the two d–d transition bands was observed in the spectrum after 24 hours which indicates the complete conversion of Ru(III) ions to Ru (0) due to reaction of *Aloe vera* gel with aqueous solution of $RuCl_3 \cdot 3H_2O$ and formation of Ru nanoparticles. The synthesis of Ru nanoparticles have already been reported
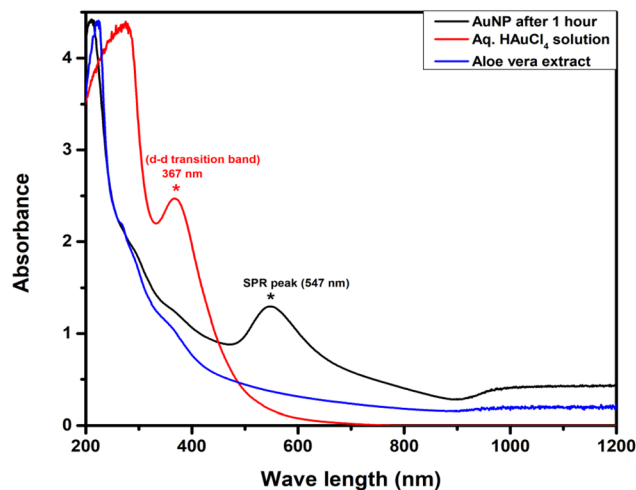
Fig. 3 UV-visible spectra of AuNPs synthesized using *Aloe vera* gel, aqueous solution of $HAuCl_4$ and *Aloe vera* extract.

using *Aloe vera* gel.[26] In the second step towards the synthesis of bimetallic Au–Ru nanoparticles, auric acid stock solution was added to the Ru nanoparticle suspension and stirred till the characteristic SPR peak of AuNPs appeared at 543 nm and the colour of the solution turned purple from dark brown. This observation is also supported by several reports.[63–66]

A slight hypsochromic displacement of the absorption band of the Au–Ru bimetallic NPs from 547 nm (Fig. 3) to 543 nm (Fig. 4) was observed indicating the formation of heterojunction bimetallic NPs of Au and Ru.

3.2 FT-IR spectroscopic analysis

The FT-IR spectrum of vacuum dried *Aloe vera* gel, AuNPs and Au–Ru NPs were recorded and compared in order to identify the possible interactions of *Aloe vera* gel with metal salts (Fig. 5). Some of the FT-IR bands in the spectrum of *Aloe vera* gel disappear while others change position or intensity
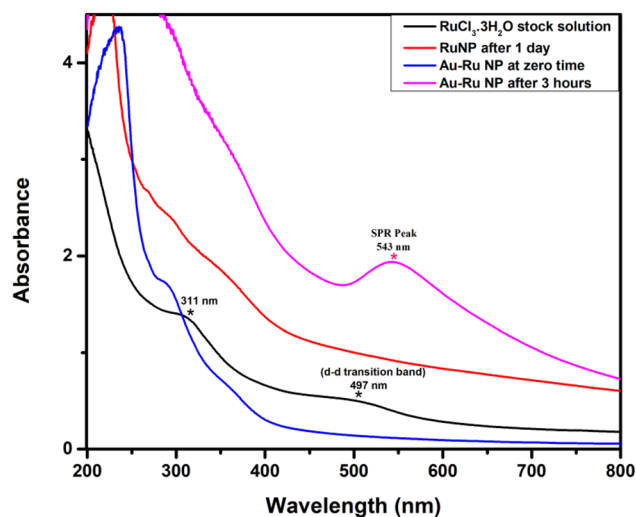
Fig. 4 UV-visible spectra of bimetallic Au–Ru NPs synthesized using *Aloe vera* gel at different time intervals.
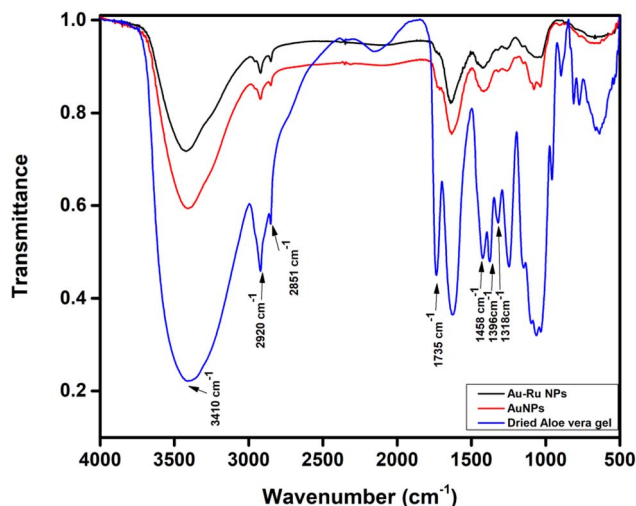
Fig. 5 FT-IR spectra of dried *Aloe vera* gel, AuNPs, and Au–Ru NPs.

after the formation of nanoparticles. Analysis of the three spectra indicates the possible role of the functional groups present in *Aloe vera* gel in reducing and stabilizing the nanoparticles.

The FTIR spectrum of *Aloe vera* gel exhibits a prominent peak at 3410 cm^{-1}, corresponding to the stretching vibration of O–H groups, which are typically present in alcohols and phenolic compounds like chrysophanol, acetylated glucomannan, acetylated mannan, arabinogalactan *etc.*[67] Two weak bands observed at approximately 2920 cm^{-1} and 2851 cm^{-1} are attributed to C–H stretching vibrations.[68] A distinct peak at 1735 cm^{-1} corresponds to the C=O stretching vibration of carbonyl compounds (*e.g.*, aloe-emodin, aloin) present in the

gel. Additional peaks at 1458.18 cm^{-1} and 1396.46 cm^{-1} are related to the symmetric bending vibrations of CH$_3$ groups. The peak observed at 1624 cm^{-1} is associated with the amide I band, characteristic of proteins and enzymes *e.g.*, aloe globulins, lectins *etc.*

Upon nanoparticle synthesis, the disappearance of the 1735 cm^{-1} peak, corresponding to carbonyl groups, indicates their involvement in the reduction of metal salts into nanoparticles. Additionally, a notable reduction in the intensity of 3410 cm^{-1} peak was observed, suggesting that phenolic compounds in *Aloe vera* also play a significant role in the reduction process and in capping and stabilizing the nanoparticles. Moreover the proteins present in the medium prevent agglomeration and stabilized the metal nanoparticles.[69,70]

The FTIR spectra of Au NPs and Au–Ru NPs are almost similar as the vibration frequencies of metal–metal bonds generally fall outside the typical range of wave number from 500 cm^{-1} to 4000 cm^{-1}.

3.3 FESEM/EDX analysis

The results of FESEM/EDX analysis of vacuum dried AuNPs are shown in Fig. 6. EDX mapping for spectrum 2 (pink rectangular selected area) with elemental composition supports the incorporation of Au nanoparticles in *Aloe vera* gel.

EDX spectrum of bimetallic Au–Ru NPs confirms the presence of Au and Ru for the selected area (Fig. 7). EDX mapping showed the distribution of metals on the surface.

3.4 HR-TEM/SAED analysis

HRTEM images of AuNPs and Au–Ru NPs at different scales are shown in Fig. 8 and 9. The results from TEM images of AuNPs
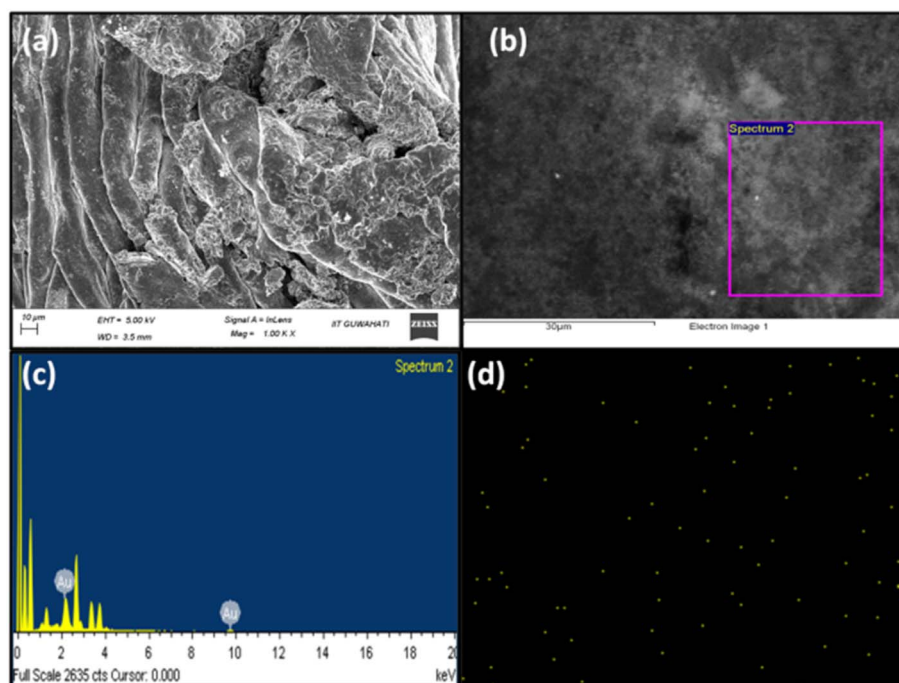

Fig. 6 (a) FE-SEM images of AuNPs, (b) selected area for mapping, (c) EDX mapping of gold nanoparticles, (d) EDX mapping of AuNPs.
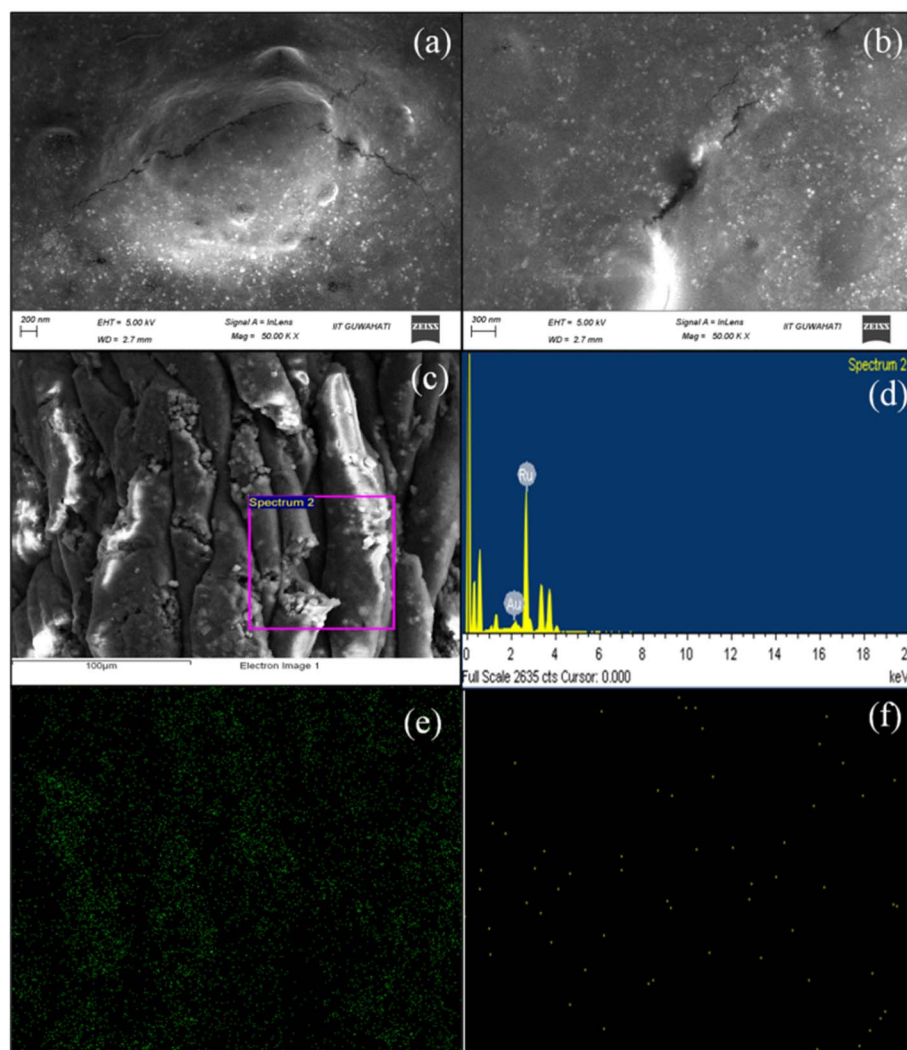
Fig. 7 (a) and (b) FE SEM images of Au–Ru NPs, (c) selected area for mapping, (d) EDX spectrum of Au–Ru NPs nanoparticles, (e) EDX mapping of Ru (f) EDX mapping of Au.

indicate that particles are predominantly spherical shaped with diameter 7.5–71.5 nm whereas some particles are tri-angular and rod shaped. Selected-area electron diffraction (SAED) pattern indicates the highly crystalline nature of the AuNPs.

HRTEM images of Au–Ru NPs at different scales confirm the formation of hexagonal bimetallic Au–Ru NPs of size in the range 19.04–76.19 nm. SAED pattern confirms the formation of crystalline Au–Ru NPs. From the two figures it can be concluded that synthesis of AuNPs using *Aloe vera* gel leads to the formation of spherical, triangular and rod shaped nanoparticles. But the synthesis of bimetallic Au–Ru NPs leads to the formation of hexagonal nanoparticles. Because, Ru nanoparticles were synthesized first using *Aloe vera* gel which lead to the formation of only hexagonal nanoparticles which is in accordance with our previous study.[26] Then gold stock solution was added to it and due to the deposition of AuNPs on the surface of Ru nanoparticles the shape is predominantly hexagonal (Fig. 9).

Moreover, the HRTEM micrographs (Fig. 9B) provide additional visual evidence for this interaction. The observed clustered or closely associated regions within the nanoparticles are consistent with the formation of a heterojuction rather than a simple physical mixture. These clusters arise due to the growth of both metal species under the same synthetic conditions, which promotes intimate contact and partial alloying at the nanoscale. Such structural arrangements are known to induce interface-mediated electronic effects, aligning well with the hypsochromic behavior observed in the UV-vis spectrum.

The crystallite size distribution graphs for the synthesized AuNPs and Au–Ru NPs are presented in Fig. 10. The mean diameters of AuNPs and Au–Ru NPs were determined to be 54.81 ± 6.11 nm and 38.30 ± 2.23 nm, respectively, which are in good agreement with the crystallite sizes calculated using the Debye–Scherrer equation. The inclusion of the distribution plots not only supports this correlation but also provides a clearer visualization of size uniformity, thereby enhancing the reliability of the results and offering deeper insight into the nucleation and growth behavior of the synthesized nanoparticles.
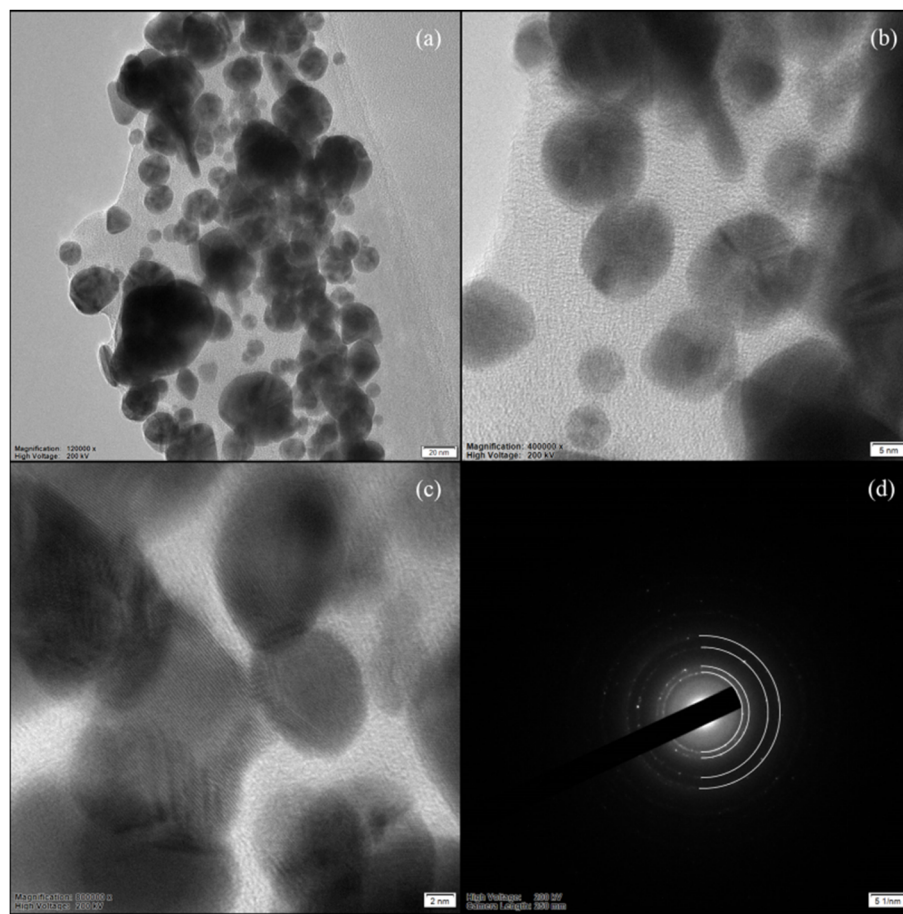
Fig. 8 HR TEM images of AuNPs (a) at 20 nm (b) at 5 nm (c) at 2 nm (d) SAED pattern of AuNPs.

3.5 Powder XRD analysis

Powder XRD analysis of vacuum dried AuNPs and Au–Ru NPs are shown in Fig. 11. Sharp peak in the XRD pattern indicates that the NPs formed are of high crystallinity. The major peaks at 2θ values of 38.11°, 44.38°, 64.71° and 77.57° for AuNPs corresponds to the lattice plane (111), (200), (220) and (311) of FCC (face centered cubic) structure of metallic Au (JCPDS no. 04-0784).The average particle size of the Au-NPs formed were calculated using Debye–Scherrer equation,

$$D = K\lambda/\beta\cos\theta \qquad (2)$$

where, D is the particle size, K is the Scherrer constant, λ is the wavelength of the X-ray radiation, β is the full width at half maximum and θ is the Bragg angle.

From the Debye–Scherrer equation average particle size of gold nanoparticles are found to be around 61 nm, which are good in agreement with TEM results also.[71–74]

The additional diffraction peaks at 29.01°, 35.77° in the Au–Ru NPs diffractogram corresponds to the planes [110], [100], for the hexagonal close packed structure of Ru nanoparticles[26] (JCPDS card no. 006-0663). Thus Au–Ru NPs diffractogram showed the presence of both Au and Ru metal. The average particle size of Au–Ru nanoparticles, calculated using the Debye–Scherrer equation, is approximately 36.49 nm, which is also consistent with the results obtained from TEM analysis.

3.6 Zeta potential

Zeta potential value of the synthesized nanoparticles was shown in Fig. 12. The zeta potential value was determined to be −5.99 mV and −12.2 mV on the surface of AuNPs and Au–Ru NPs, respectively. The zeta potential values give us the information regarding the surface charge of nanoparticles which appeared to be negative here.

Singh *et al.* reported the synthesis of gold and silver nanoparticles using *Panax ginseng* fresh leaf extract, demonstrating colloidal stability characterized by negative surface charges of approximately −16.0 mV for gold nanoparticles and −19.3 mV for silver nanoparticles.[75] In a related study, Singh and her colleagues synthesized gold and silver nanoparticles from *Euphrasia officinalis* leaf extract. The zeta potential values were measured as −22.4 ± 2.1 mV for silver nanoparticles and −15.0 ± 1.5 mV for gold nanoparticles, further indicating good stability due to electrostatic repulsion on the nanoparticle surfaces[76] (Fig. 12).

3.7 Cytotoxic assay

The trypan blue exclusion assay is a powerful tool for evaluating the cytotoxic effects of potential anticancer agents on cultured cancer cells. By quantifying the number of stained (dead) cells post-treatment, researchers can gain insights into the efficacy of
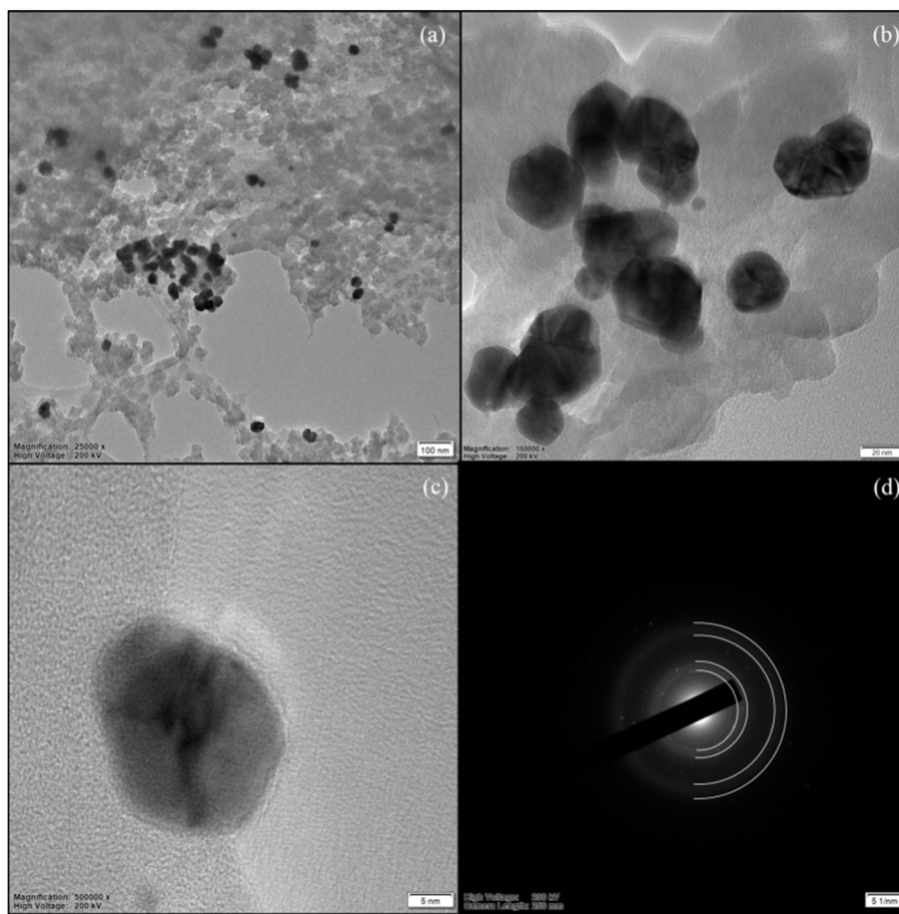
Fig. 9 HR TEM images of Au–Ru NPs (a) image at 100 nm (b) image at 20 nm (c) image at 5 nm (d) SAED pattern of Au–Ru NPs.
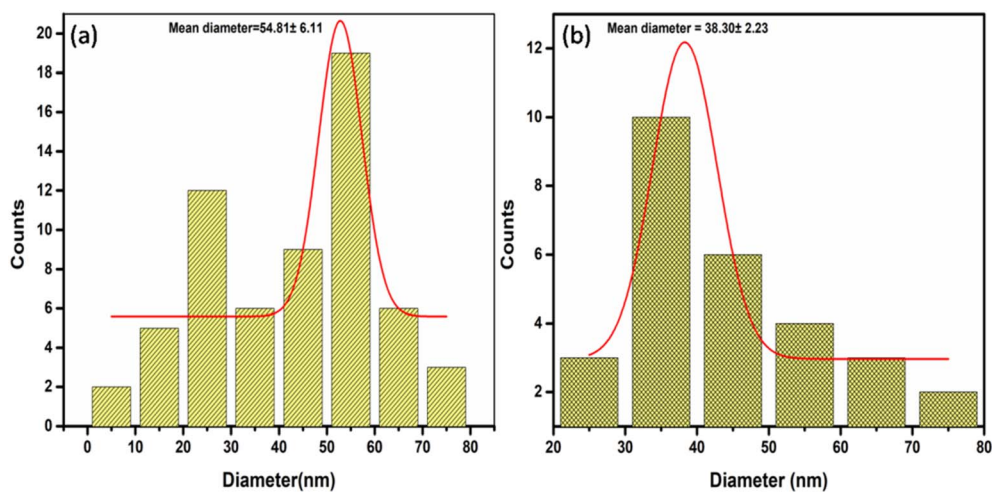

Fig. 10 Crystallite size distribution graph (a) AuNPs (b) Au–Ru NPs.

specific drug candidates. This technique is based on the differential permeability of the trypan blue dye, where live cells with intact membranes exclude the dye, while dead cells allow it to penetrate and exhibit a blue coloration.[77]

Microscopic examination of untreated control cells revealed a characteristic round shape indicative of healthy cells with intact membranes, providing a baseline for comparison with treated cells. In contrast, treated cells exhibited significant morphological changes under high magnification after trypan blue staining, including chromatin condensation and membrane damage (Fig. 13). Chromatin condensation is often
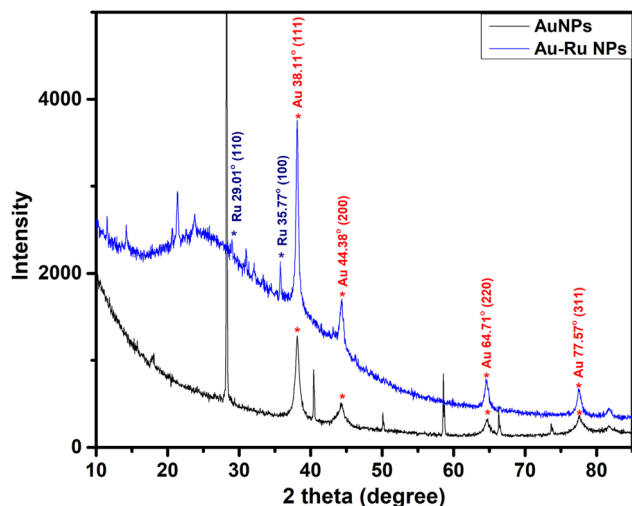
Fig. 11 Powder-XRD of AuNPs and Au-RuNPs.

associated with apoptosis, suggesting that Au–Ru NP and AuNP may induce programmed cell death in cancer cells.

The cytotoxicity result (Fig. 14) illustrates the cytotoxic effects of cisplatin, ALV gel, Au–Ru NP, and AuNP on the DL cancer cell line and PBMC normal healthy cell line after 48 hours of treatment. Cisplatin demonstrated the highest cytotoxicity against DL cancer cells across all doses tested, with a pronounced increase in effectiveness as the dose increased. ALV gel exhibited low cytotoxicity in DL cancer cells that increased with dose but remained less effective than cisplatin. Au–Ru NP showed significant cytotoxicity at higher doses (5 μM and 10 μM), marked by an asterisk indicating significance compared to AuNP. Meanwhile, AuNP displayed moderate cytotoxicity in DL cancer cells relative to other treatments.In PBMC normal cells, ALV gel and Au–Ru NP exhibited minimal cytotoxicity (~10%) across all doses, indicating their relative safety for normal cells. Notably, AuNP showed very low or negligible cytotoxicity in PBMC normal cells, suggesting it is the least harmful to healthy tissues among the treatments. These findings underscore the differential effects of these anticancer agents on cancerous *versus* healthy cell lines;

cisplatin emerged as the most potent against cancer cells while ALV gel and Au–Ru NP demonstrated potential for selective targeting with minimal impact on normal cells. The simple linear regression (Table 1) analysis after 48 hours of treatment revealed significant dose-dependent cytotoxicity across all four treatments in both DL and PBMC cell lines ($P < 0.01$), with excellent model fit ($R^2 > 0.61$). Notably, all treatments demonstrated substantially higher slopes in the DL cancer cell line (cisplatin: 11.53, Au–Ru NP: 7.471, AuNP: 5.771, ALV gel: 3.286) compared to the PBMC normal cells (0.7429, 1.057, 0.5400 respectively), indicating selective cytotoxicity toward cancer cells.

The IC$_{50}$ values (Fig. 15) for cisplatin (reference drug), ALV gel, Au–Ru NP, and AuNP after 48 hours of treatment in the DL cell line revealed significant differences in their potency. Cisplatin had an IC$_{50}$ value of 0.49 ± 0.27 μM, indicating high effectiveness at low concentrations. In contrast, ALV gel presented a very high IC$_{50}$ value of 989.4 ± 0.02 μM, suggesting that it is much less effective than other treatments. Au–Ru NP had an IC$_{50}$ value of 18.34 ± 0.02 μM showing highest potency, while AuNP's IC$_{50}$ value of 46.7 ± 0.018 μM indicated it was moderate potent than both ALV gel and Au–Ru NP but more effective than ALV gel. These results highlight varying degrees of effectiveness in inhibiting cell viability in the DL cell line, positioning Au–Ru NP as the most promising candidate for further study.

Based on the simple linear regression analysis (Table 2) of cytotoxicity after 48 hours of treatment in the DL cell line, all four experimental groups demonstrated strong dose-dependent relationships with highly significant P values (<0.0001) and excellent goodness-of-fit ($R^2 > 0.89$). Cisplatin exhibited the steepest slope (18.81), indicating the highest cytotoxic potency, followed by Au–Ru NP (14.05), AuNP (11.31) and ALV gel (7.435), suggesting that cisplatin produces the greatest increase in cytotoxicity per unit dose increase, while ALV gel shows the most gradual dose–response effect.

Interestingly, cytotoxicity studies revealed minimal impact (<10%) on non-cancerous PBMC cell lines for ALV gel, Au–Ru NP, and AuNP (Fig. 13). This suggests a degree of selectivity for cancer cellsan ideal characteristic for potential therapeutic
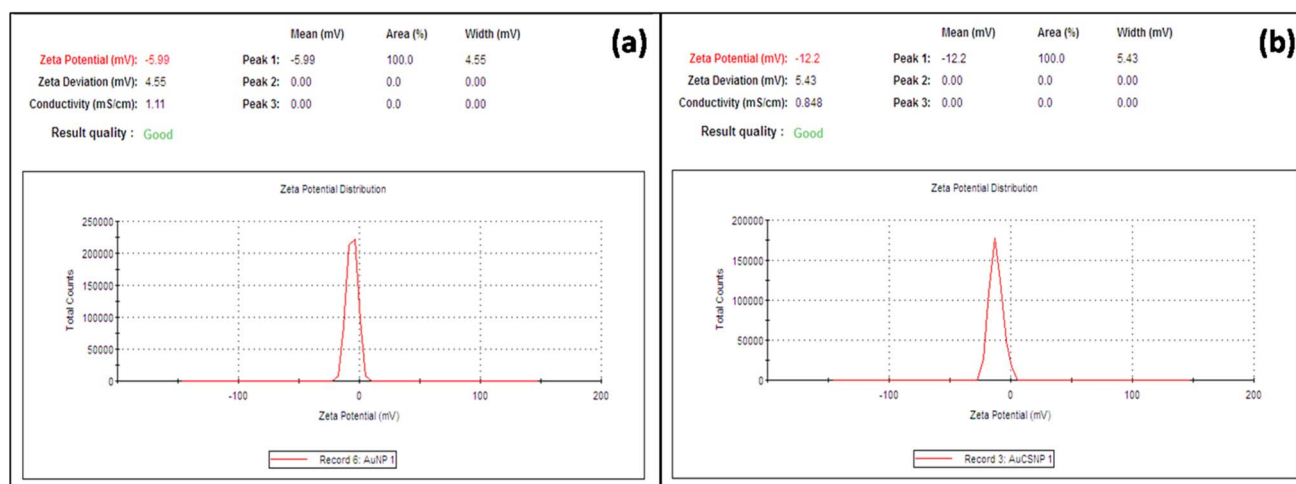

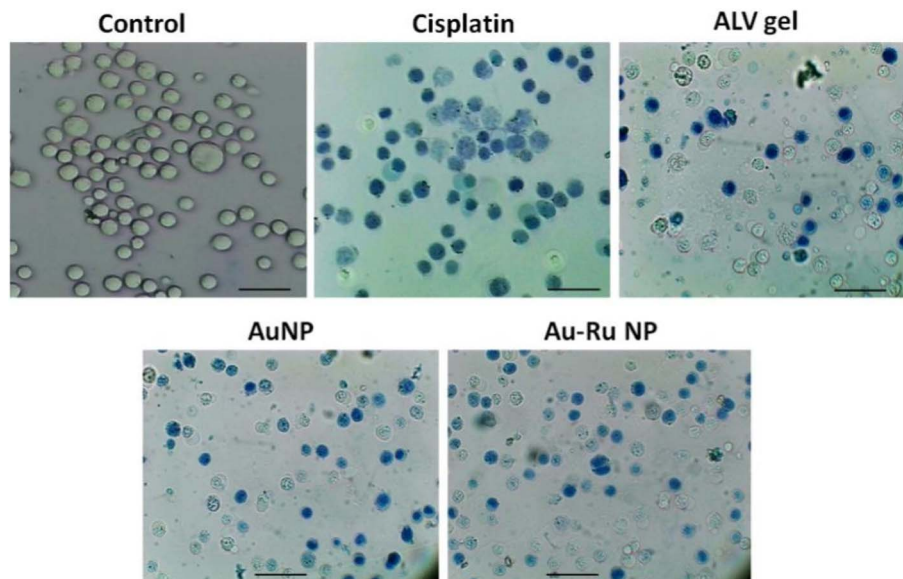Fig. 12 Zeta potential values of (a) AuNPs and (b) Au−Ru NPs synthesized from *Aloe vera* gel.

Fig. 13 Microscopic evaluation of trypan blue-stained DL cells following 48 h treatment (dose; 10 μM). Blue stained cells represent dead cells with compromised membranes, whereas unstained cells indicate live cells with intact membranes. Scale bar: 20 μm.
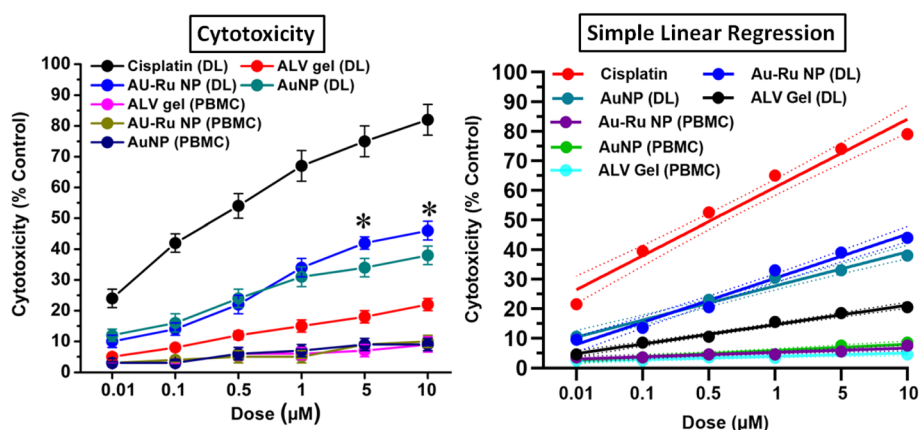

Fig. 14 Percentage cytotoxicity (left) of cisplatin, ALV gel, Au–Ru NP and AuNP after 48 hours of treatment in the Dalton's lymphoma (DL) and non-cancerous (PBMC) cell lines. Simple linear regression (right) showed time dependent increase in cytotoxicity. Data are mean ± S.D., $n = 3$, One way ANOVA, *$P \leq 0.05$ as compared to AuNP.

agents aiming to target tumors while minimizing harm to healthy tissues. The observed low cytotoxicity of Au–Ru NP and AuNP in PBMCs warrants further investigation to elucidate the mechanisms underlying this selectivity.

The ingredients of *Aloe vera* gel are already reported effective for the synthesis of metal nanoparticles.[26] The synthesis of Au NPs and the bimetallic AuRu NPs was done following the same procedure so that a perfect comparison of the two types of NPs

Table 1 Simple linear regression analysis details of cisplatin, Au–Ru NP, AuNP and ALV gel after 48 hours of treatment in both DL and PBMC cell lines

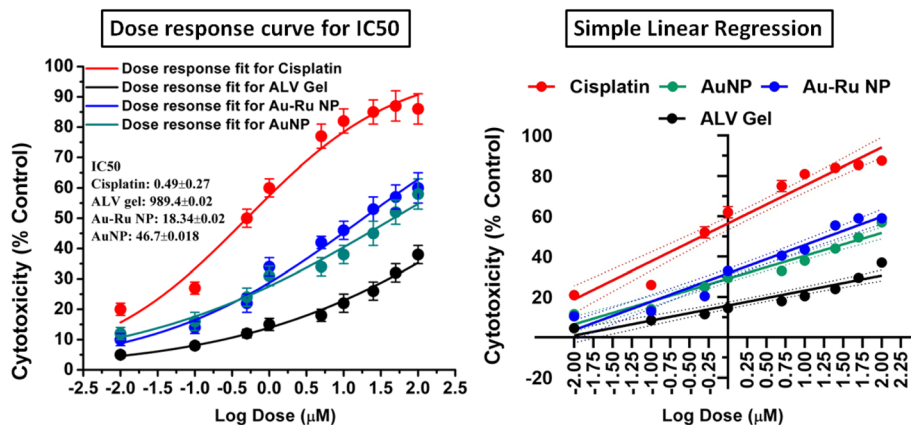| Parameters	Experimental groups						
	Cisplatin (DL)	Au–Ru NP (DL)	AuNP (DL)	ALV gel (DL)	Au–Ru NP (PBMC)	AuNP (PBMC)	ALV gel (PBMC)
Slope	11.53	7.471	5.771	3.286	0.7429	1.057	0.5400
Equation	$Y = 11.53 \times X + 14.90$	$Y = 7.471 \times X + 0.4333$	$Y = 5.771 \times X + 4.633$	$Y = 3.286 \times X + 1.500$	$Y = 0.7429 \times X + 2.233$	$Y = 1.057 \times X + 1.633$	$Y = 0.5400 \times X + 1.760$
R squared	0.9654	0.9745	0.9670	0.9789	0.7525	0.8037	0.6159
P Value	<0.0001	<0.0001	<0.0001	<0.0001	0.0003	<0.0001	0.0025

Fig. 15 The *in vitro* IC_{50} values for cisplatin, ALV gel, Au–Ru NPs and AuNPs after 48 hours of treatment in the DL cell line demonstrate significant differences in their potency (left). Simple linear regression (right) showed time dependent increase in cytotoxicity. Data are mean $\pm$ S.D., $n = 3$.

Table 2 Simple linear regression analysis details of cisplatin, Au–Ru NP, AuNP and ALV gel after 48 hours of treatment in the DL cell line

Parameters	Experimental groups			
	Cisplatin	Au–Ru NP	AuNP	ALV gel
Slope	18.81	14.05	11.31	7.435
Equation	$Y = 18.81 \times X + 56.47$	$Y = 14.05 \times X + 31.71$	$Y = 11.31 \times X + 29.11$	$Y = 7.435 \times X + 15.78$
R squared	0.9417	0.9440	0.9459	0.8986
P Value	<0.0001	<0.0001	<0.0001	<0.0001

Table 3 Comparison of earlier reported bimetallic NPs and current biosynthesized bimetallic NPs

Plant extract	Metals	Synthesis conditions	Size/shape	Application	References
Honey and *Gymnema sylvestre* leaf extract	Au	20–70 °C	20 to 50 nm, large-sized nanocubes	Cytotoxicity study on MCF7 and MDA-MB-231 cells	25
Andrographis paniculata, *Acalypha indica*	Ag–Au	Room temparature, 24 hours	25 to 50 nm, mostly spherical shape	Antimycobacterial efficacy	50
Croton Caudatus Geisel	Au–Pt	60 °C	12 to 33 nm, rectangular shaped	Cytotoxicity study on HeLa cancer cells	46
Gloriosa superba leaf extract	Ag–Au	50–60 °C	Approx 20 nm, triangular and spherical shaped	Antibacterial activity on gram (+) and gram (−) bacteria	18
Rosemary and ginseng extracts	Pd–Pt	100 °C, 3 hours	Approximately 3.7 ± 0.8 nm also larger and smaller size varies, spherical	Cytotoxicity study on colon cancer cell lines (Ls180, SW480)	20
Aloe vera	**Au–Ru**	**Room temparature, 3 hour**	**Hexagonal**	**Cytotoxicity study on DL cell lines**	**Present study**

can be done while investigating their anticancer activities in DL-cell line. Moreover, the *Aloe vera* gel used to synthesize the two types of NPs was itself investigated for its own anticancer potential for more accurate results. The bimetallic nanoparticles were synthesized with an aim to use the synergistic effect of Au and Ru metals. Gold NPs are known for their excellent biocompatibility and optical properties while ruthenium NPs have shown strong strong anticancer properties because of their ability to mimic iron and interact with DNA.[78] There are several bimetallic nanoparticles reported to show their anticancer potential in MCF-7, HT-29, HCT-116, HeLa and A-549 cell lines[23,79,80]. But there are only two reports available in

the literature on the synthesis of Au–Ru bimettalic nanoparticles. A sonochemical synthesis of Au–Ru nanoparticles has been reported by Panneer Selvam *et al.*[28]. Shabani *et al.*[81] have also reported the synthesis of Ru template gold nanoparticles using rutin extract and their findings demonstrate the significant efficacy of Ru–Au NPs coupled with laser radiation in the treatment of breast cancer MCF-7 cells. But our work is the first showcase of a phytogenic synthesis of Au–Ru bimetallic nanoparticles and investigation of their anticancer activity in DL cell line through trypan blue assay. The IC_{50} value of Au–Ru bimettallic NPs is lower than the monometallic Ru NPs[26] or Au NPs alone. The bimetallic NPs, therefore, exhibit enhanced

anticancer potency which may be due to synergistic effect, targeted specificity through reactive oxygen species (ROS) generation, mitochondrial dysfunction and triggering the apoptotic pathways in cancer cells.[32]

Compared with other plant extracts, *Aloe vera* demonstrates superior efficiency for the synthesis of bimetallic metal nanoparticles. Notably, the Au–Ru nanoparticles in the present study were synthesized under mild conditions whereas many reported systems require elevated temperatures and prolonged durations. This efficiency may be attributed to the rich phytochemical profile of *Aloe vera*, including polysaccharides, phenolics, flavonoids, and organic acids, which can simultaneously facilitate metal ion reduction and nanoparticle stabilization. A comparative analysis of different plant-based nanoparticle fabrication methods is presented in Table 3.

4 Conclusion

The present study demonstrates the successful biogenic synthesis of Au–Ru bimetallic nanoparticles through a green, successive growth-mediated approach using *Aloe vera* gel as a reducing and stabilising agent. The characterization of the synthesized NPs using UV-vis spectrophotometry, FT-IR, HR-TEM, powder XRD, and FESEM/EDX confirmed the formation of the bimetallic Au–Ru NPs with hexagonal shape. The average particle size of Au–Ru nanoparticles was found to be 36.49 nm, which is also consistent with the results obtained from TEM analysis. The bimetallic Au–Ru nanoparticles exhibited enhanced anticancer activity in DL cell line compared to monometallic AuNPs and *Aloe vera* gel as demonstrated by the Trypan Blue assay and IC_{50} values. The cytotoxicity studies also revealed negligible effect of the bimetallic nanoparticles on non-cancerous PBMC cell lines. Thus, Au–Ru bimetallic NPs present a promising nano platform for cancer therapy. Although the present work primarily focuses on the anti cancer potential of Au–Ru bimettalic nanoparticles on DL cancer cell line and does not include mechanistic or *in vivo* evaluations, these aspects provide clear and valuable directions for further research. Building on the promising outcomes observed in this studies, future studies will aim to elucidate the underlying molecular mechanisms and extend the evaluation in different cancer cell lines. These efforts will further strengthen the therapeutic relevance of Au–Ru bimetallic nanoparticles and support their advancement toward applications in photothermal therapy and diagnostic imaging.

Author contributions

Tanjila Begum – investigation, conceptualization, methodology, data curation, formal analysis, visualisation, writing – original draft. Sangeeta Agarwal – methodology, supervision, conceptualization, writing – review & editing. Pranab Borah – investigation, methodology, data curation. Akalesh Kumar Verma – formal analysis, methodology, resources, supervision, writing – original draft, writing – review & editing. Arundhuti Devi – data curation, formal analysis, methodology, visualisation, writing – review & editing. Mausumi Ganguly – supervision, project administration, resources, writing – review & editing.

Conflicts of interest

There are no conflicts to declare.

Abbreviations

DL Cell	Dalton's lymphoma cell
AuNPs	Gold nanoparticles
Au–Ru NPs	Gold–Ruthenium bimetallic nanoparticles

Data availability

The data supporting this article have been included as part of the supplementary information (SI). Supplementary information is available. See DOI: https://doi.org/10.1039/d5ra08541a.

References

1 R. Seigneuric, L. Markey, D. S. Nuyten, C. Dubernet, C. T. Evelo, E. Finot and C. Garrido, *Curr. Mol. Med.*, 2010, **10**(7), 640–652, DOI: 10.2174/156652410792630634.

2 W. H. Gmeiner and S. Ghosh, *Nanotechnol. Rev.*, 2015, **3**(2), 111–122, DOI: 10.1515/ntrev-2013-0013.

3 X. Wang, Y. Wang, Z. G. Chen and D. M. Shin, *Cancer Res. Treat.*, 2009, **41**(1), 1–11, DOI: 10.4143/crt.2009.41.1.1.

4 H. Lan, M. Jamil and G. Ke, *Am. J. Cancer Res.*, 2023, **13**(12), 5751–5784.

5 Q. Zhou, L. Zhang and H. Wu, *Nanotechnol. Rev.*, 2017, **6**, 473–496, DOI: 10.1515/ntrev-2016-0102.

6 Y. Lu, D. Zhu, Q. Le, Y. Wang and W. Wang, *Nanoscale*, 2022, **14**, 16339–16375.

7 C. Kher and S. Kumar, *Cureus*, 2022, **14**(9), 29059, DOI: 10.7759/cureus.29059.

8 G. Zhang, X. Zeng and P. Li, *J. Biomed. Nanotechnol.*, 2013, **9**(5), 741–750, DOI: 10.1166/jbn.2013.1583.

9 Z. Cheng, M. Li, R. Dey and Y. Chen, *J. Hematol. Oncol.*, 2021, **14**(1), 85, DOI: 10.1186/s13045-021-01096-0.

10 Y. Zhou, M. Xu, Y. Liu, Y. Bai, Y. Deng, J. Liu and L. Chen, *Colloids Surf. B Biointerfaces*, 2016, **144**, 118–124, DOI: 10.1016/j.colsurfb.2016.04.004.

11 K. A. Elsayed, M. Alomari, Q. A. Drmosh, M. Alheshibri, A. Al, T. S. Kayed, A. A. Manda and A. L. Al-alotaibi, *Alex. Eng. J.*, 2022, **61**(2), 1449–1457, DOI: 10.1016/j.aej.2021.06.051.

12 I. Shmarakov, I. Mukha, N. Vityuk, V. Borschovetska, N. Zhyshchynska, G. Grodzyuk and A. Eremenko, *Nanoscale Res. Lett.*, 2017, **12**(1), 1–10.

13 H. Katifelis, I. Mukha, P. Bouziotis, N. Vityuk, C. Tsoukalas, A. C. Lazaris, A. Lyberopoulou, G. E. Theodoropoulos, E. P. Efstathopoulos and M. Gazouli, *Int. J. Nanomed.*, 2020, **15**, 6019–6032, DOI: 10.2147/IJN.S251760.

14 J. Gomez-Bolivar, I. P. Mikheenko, R. L. Orozco, S. Sharma, D. Banerjee, M. Walker, R. A. Hand, M. L. Merroun and L. E. Macaskie, *Front. Microbiol.*, 2019, **10**, 1276, DOI: 10.3389/fmicb.2019.01276.

15 J. B. Omajali, J. Gomez-Bolivar, I. P. Mikheenko, S. Sharma, B. Kayode, B. Al-duri, D. Banerjee, M. Walker, M. L. Merroun and L. E. Macaskie, *Sci. Rep.*, 2019, **9**, 1–12, DOI: 10.1038/s41598-019-40312-3.

16 S. Ghosh, R. Nitnavare, A. Dewle, G. B. Tomar, R. Chippalkatti, P. More, R. Kitture, S. Kale, J. Bellare and B. A. Chopade, *Int. J. Nanomed.*, 2015, **10**, 7477–7490, DOI: 10.2147/IJN.S91579.

17 N. O. Alafaleq, T. A. Zughaibi, N. R. Jabir, A. U. Khan, M. S. Khan and S. Tabrez, *Nanomaterials*, 2023, **13**(7), 1201, DOI: 10.3390/nano13071201.

18 K. Gopinath, S. Kumaraguru, K. Bhakyaraj, S. Mohan, K. S. Venkatesh, M. Esakkirajan, P. Kaleeswarran, N. S. Alharbi, S. Kadaikunnan, M. Govindarajan, G. Benelli and A. Arumugam, *Microb. Pathog.*, 2016, **101**, 1–11, DOI: 10.1016/j.micpath.2016.10.011.

19 P. K. Jha, T. Jaidumrong, D. Rokaya and C. Ovatlarnporn, *RSC Adv.*, 2024, **14**, 11017–11026, DOI: 10.1039/d4ra01355g.

20 B. Sundaram, V. Sri, G. Archunan, C. Chaiyasut and N. Suganthy, *J. Drug Deliv. Sci. Technol.*, 2019, **51**, 139–151, DOI: 10.1016/j.jddst.2019.02.024.

21 H. Katifelis, A. Lyberopoulou, I. Mukha, N. Vityuk, G. Grodzyuk, G. E. Theodoropoulos, E. P. Efstathopoulos and M. Gazouli, *Artif. Cells, Nanomed. Biotechnol.*, 2018, **46**(sup3), S389–S398, DOI: 10.1080/21691401.2018.1495645.

22 F. Gulbagça, A. Aygun, E. E. Altuner, M. Bekmezci, T. Gur, F. Sen, H. Karimi-Maleh, N. Zare, F. Karimi and Y. Vasseghian, *Chem. Eng. Res. Des.*, 2022, **180**, 254–264.

23 J. J. Martínez-Sanmiguel, D. Zarate-Triviño, M. P. García-García, J. M. García-Martín, Á. Mayoral, Y. Huttel, L. Martínez and J. L. Cholula-Díaz, *RSC Adv.*, 2024, **14**(53), 39102–39111, DOI: 10.1039/d4ra06227b.

24 G. Unnikrishnan, A. Joy, M. Megha, E. Kolanthai and M. Senthilkumar, *Discover Nano*, 2023, **18**, 157, DOI: 10.1186/s11671-023-03943-0.

25 S. Malik, M. Niazi, M. Khan, B. Rauff, S. Anwar, F. Amin and R. Hanif, *ACS Omega*, 2023, **8**, 6325–6336.

26 T. Begum, S. Agarwal, P. Bhuyan, J. Das, A. Kumar, A. Guha, M. Ganguly and K. Words, *Nanotechnol.*, 2025, **7**, 100095, DOI: 10.1016/j.nxnano.2024.100095.

27 S. Y. Lee, C. Y. Kim and T. G. Nam, *Drug Des., Dev. Ther.*, 2020, **14**, 5375–5392, DOI: 10.2147/DDDT.S275007.

28 P. Selvam, A. Manivel, S. Anandan, M. Zhou, F. Grieser and M. Ashok kumar, *Colloids Surf. A Physicochem. Eng. Asp.*, 2010, **356**(1–3), 140–144, DOI: 10.1016/j.colsurfa.2010.01.004.

29 L. Boselli, M. Carraz, S. Mazères, L. Paloque, G. González, F. Benoit-Vical, A. Valentin, C. Hemmert and H. Gornitzka, *Organometallics*, 2015, **34**(6), 1046–1055.

30 O. A. Kirichenko, E. A. Redina, N. A. Davshan, I. V. Mishin, G. I. Kapustin, T. R. Brueva, L. M. Kustov, W. Li and C. H. Kim, *Appl. Catal. B Environ.*, 2013, **134**, 123–129.

31 K. F. Chernysheva and A. A. Revina, *Russ. J. Phys. Chem. B*, 2019, **13**(3), 452–457, DOI: 10.1134/S1990793119030023.

32 L. A. Calzada, S. E. Collins, C. W. Han, V. Ortalan and R. Zanella, *Appl. Catal. B Environ.*, 2017, **207**, 79–92, DOI: 10.1016/j.apcatb.2017.01.081.

33 L. E. Chinchilla, C. Olmos, M. Kurttepeli, S. Bals, G. Van Tendeloo, A. Villa, L. Prati, G. Blanco, J. J. Calvino, X. Chen and A. B. Hungría, *Part. Part. Syst. Charact.*, 2016, **33**(10), 1–10, DOI: 10.1002/ppsc.201600057.

34 M. Khalid, X. Zarate, M. Saavedra-Torres, E. Schott, A. M. Honorato, B. Rafe, H. Varela and M. A. Varela, *Chem. Eng. J.*, 2021, **421**(1), 129987, DOI: 10.1016/j.cej.2021.129987.

35 Madhukriti, A. Roy, S. Pandit, A. Kumar, K. Sharma, S. Raj, V. Raja and H. Y. Setyawan, *BioNanoScience*, 2025, **15**, 351, DOI: 10.1007/s12668-025-01913-7.

36 S. Bhusari, P. M. Sah, J. Lakkakula, A. Roy, R. Raut, R. Chondekar, S. Alghamdi, M. Almehmadi, M. Allahyani, A. A. Alsaiari, A. Aljuaid and N. Al-Abdullah, *Green Process. Synth.*, 2023, **12**, 20230051, DOI: 10.1515/gps-2023-0051.

37 A. Kumar, T. Siddiqui, S. Pandit, A. Roy, A. Gacem, A. A. Souwaileh, A. S. Mathuriya, T. Fatma, P. Sharma, S. Rustagi, K. K. Yadav, B. H. Jeon and H. K. Park, *Catalysts*, 2023, **13**, 937, DOI: 10.3390/catal13060937.

38 A. Michael, A. Singh, R. Mishra, A. Roy, A. Roy, K. Kaur, S. Rustagi, S. Malik, R. Verma and K. Sharma, *Nano-Struct. Nano-Objects*, 2024, **38**, 101190, DOI: 10.1016/j.nanoso.2024.101190.

39 D. S. Idris, A. Roy, A. Malik, A. A. Khan, K. Sharma and A. Roy, *J. Inorg. Organomet. Polym.*, 2025, **35**, 594–606, DOI: 10.1007/s10904-024-03316-9.

40 V. M. Canh, S. Ghotekar, N. M. Viet, H. Dabhane, R. Oza and A. Roy, *Plant and Nanoparticles*, Springer, Singapore, 2022, DOI: 10.1007/978-981-19-2503-0_13.

41 V. K. Chaturvedi, N. Yadav, N. K. Rai, R. A. Bohara, S. N. Rai, L. Aleya and M. P. Singh, *Environ. Sci. Pollut. Res. Int.*, 2021, **28**(11), 13761–13775, DOI: 10.1007/s11356-020-11435-2.

42 F. J. Morales Santos, H. A. Piñón Castillo, A. Quintero-Ramos, G. Zaragoza Galán, R. Durán and E. Orrantia Borunda, *Appl. Nanosci.*, 2022, **12**(10), 2901–2913, DOI: 10.1007/s13204-022-02601-8.

43 K. Gopinath, S. Kumaraguru, K. Bhakyaraj, S. Mohan, K. S. Venkatesh, M. Esakkirajan, P. R. Kaleeswarran, S. A. Naiyf, S. Kadaikunnan, M. Govindarajan, G. Benelli and A. Arumugam, *Microb. Pathog.*, 2016, **100**, 124–133, DOI: 10.1016/j.micpath.2016.10.011.

44 R. Velamakanni, S. Ajmera, B. Nageshwari and A. Kumar, *Afr. J. Biol. Sci.*, 2024, **6**, 4670–4681, DOI: 10.48047/AFJBS.6.Si4.2024.4670-4681.

45 G. Thirumoorthy, B. Balasubramanian, J. A. George, A. Nizam, P. Nagella, N. Srinatha, M. Pappuswamy, A. M. Alanazi, A. Meyyazhagan, K. R. R. Rengasamy and V. V. Lakshmaiah, *Sci. Rep.*, 2024, **14**(1), 1–15, DOI: 10.1038/s41598-024-51647-x.

46 P. V. Kumar, K. S. Pushpavalli, B. G. Kumar, S. M. Jelastin Kala and K. S. Prakash, *Results Chem.*, 2025, **13**, 101945, DOI: 10.1016/j.rechem.2024.101945.

47 A. Surjushe, R. Vasani and D. Saple, *Indian J. Dermatol.*, 2008, **53**(4), 163–166, DOI: 10.4103/0019-5154.44785.

48 T. Reynolds and A. C. Dweck, *J. Ethnopharmacol.*, 1999, **68**(1–3), 3–37, DOI: 10.1016/S0378-8741(99)00085-9.

49 E. V. Christaki and P. C. Florou-Paneri, *J. Food, Agric. Environ.*, 2010, **8**(2), 245–249.

50 G. Ramalingam, G. Saminathan and E. Manickan, *J. Primeasia.*, 2021, **2**(1), 1–8, DOI: 10.25163/primeasia.2120218.

51 G. Mamatha, A. V. Rajulu and K. Madhukar, *J. Nat. Fibers*, 2018, 1–9, DOI: 10.1080/15440478.2018.1558146.

52 J. Karimi and S. Mohsenzadeh, *Synth. React. Inorg., Met.-Org., Nano-Met. Chem.*, 2015, **45**(6), 895–898, DOI: 10.1080/15533174.2013.862644.

53 G. Sangeetha, S. Rajeshwari and R. Venckatesh, *Mater. Res. Bull.*, 2011, **46**(12), 2560–2566, DOI: 10.1016/j.materresbull.2011.07.046.

54 K. Logaranjan, A. J. Raiza, S. C. B. Gopinath, Y. Chen and K. Pandian, *Nanoscale Res. Lett.*, 2016, **11**(1), 1–9, DOI: 10.1186/s11671-016-1725-x.

55 K. G. Rao, C. H. Ashok, K. V. Rao, C. H. S. Chakra and P. Tambur, *Int. J. Adv. Res. Phys. Sci.*, 2016, **2**, 28–34.

56 R. Gangwar, K. T. Rao, S. Khatun, A. K. Rengan, C. Subrahmanyam and S. R. Krishna Vanjari, *Appl. Nanosci.*, 2025, **15**, 18, DOI: 10.1007/s13204-025-03086-x.

57 G. Klein, *Exp. Cell Res.*, 1951, **2**(3), 518–573, DOI: 10.1016/0014-4827(51)90038-9.

58 K. Raj Kumar, *Int. J. Immunother. Cancer Res.*, 2017, **3**, 001–006, DOI: 10.17352/2455-8591.000011.

59 J. Pourahmad and A. Salimi, *Iran. J. Pharm. Res.*, 2015, **14**, 679–980.

60 D. Dutta, N. S. Singh, R. Aggarwal and A. K. Verma, *Anti Cancer Agents Med. Chem.*, 2024, **24**(9), 668–690.

61 M. Devi, A. K. Verma, N. S. Singh, J. Das, K. Dutta, M. Gogoi, D. Dutta and A. Tradit, *Med*, 2023, 1–13.

62 W. Strober, *Curr. Protoc. Immunol.*, 2015, **111**(1), A3–B.

63 Y. Shang, C. Min, J. Hu, T. Wang, H. Liu and Y. Hu, *Solid State Sci.*, 2013, **15**, 17–23, DOI: 10.1016/j.solidstatesciences.2012.09.002.

64 S. Dursun, E. Yavuz and Z. Çetinkaya, *RSC Adv.*, 2019, **9**(66), 38538–38546, DOI: 10.1039/c9ra08822a.

65 M. Ramli, I. Sujoko, N. Adhha, D. Annas, M. Nikmatullah, H. A. Ariyanta, D. O. B. Apriandanu, I. S. Saputra and K. Khairurrijal, *Results Surf. Interfaces*, 2024, **17**, 100317, DOI: 10.1016/j.rsurfi.2024.100317.

66 T. Wu, X. Duan, C. Hu, C. Wu, X. Chen, J. Huang, J. Liu and S. Cui, *Artif. Cells, Nanomed. Biotechnol.*, 2019, **47**(1), 512–523, DOI: 10.1080/21691401.2018.1560305.

67 T. Muralikrishna, M. Pattanayak and P. L. Nayak, *World J. Nano Sci. Technol.*, 2014, **3**(2), 45–51.

68 S. Medda, A. Hajra, U. Dey, P. Bose and N. K. Mondal, *Appl. Nanosci.*, 2015, **5**, 875–880.

69 S. P. Chandran, M. Chaudhary, R. Pasricha, A. Ahmad and M. Sastry, *Biotechnol. Prog.*, 2006, **22**(2), 577–583, DOI: 10.1021/bp0501423.

70 T. R. Anju, S. Parvathy, M. V. Veettil, J. Rosemary, T. H. Ansalna, M. M. Shahzabanu and S. Devika, *Mater. Today: Proc.*, 2020, **43**, 3956–3960, DOI: 10.1016/j.matpr.2021.02.665.

71 S. Malik, M. Niazi, M. Khan, B. Rauff, S. Anwar, F. Amin and R. Hanif, *ACS Omega*, 2023, **8**(7), 6325–6336, DOI: 10.1021/acsomega.2c06491.

72 B. Sadeghi, M. Mohammadzadeh and B. Babakhani, *J. Photochem. Photobiol. B Biol.*, 2015, **148**, 101–106, DOI: 10.1016/j.jphotobiol.2015.03.025.

73 T. Y. Suman, S. R. Radhika Rajasree, R. Ramkumar, C. Rajthilak and P. Perumal, *Spectrochim. Acta, Part A*, 2014, **118**, 11–16, DOI: 10.1016/j.saa.2013.08.066.

74 S. A. Aromal and D. Philip, *Spectrochim. Acta, Part A*, 2012, **97**, 1–5.

75 P. Singh, H. Singh, S. Ahn, V. Castro-Aceituno, Z. Jiménez, S. Y. Simu, Y. J. Kim and D. C. Yang, *Artif. Cells, Nanomed. Biotechnol.*, 2017, **45**(7), 1415–1424, DOI: 10.1080/21691401.2016.1243547.

76 H. Singh, J. Du, P. Singh and T. H. Yi, *Artif. Cells, Nanomed. Biotechnol.*, 2018, **46**, 1163–1170, DOI: 10.1080/21691401.2017.1362417.

77 S. Adhikari, S. Nath, S. Kansız, N. Balidya, A. K. Paul, N. Dege, O. Sahin, G. Mahmoudi, A. K. Verma and D. A. Safin, *J. Inorg. Biochem.*, 2024, 112598.

78 S. Swaminathan, J. Haribabu and R. Karvembu, *ChemMedChem*, 2024, **19**(23), e202400435, DOI: 10.1002/cmdc.202400435.

79 M. S. Alwhibi, K. M. O. Ortashi, A. A. Hendi, M. A. Awad, D. A. Soliman and M. El-Zaidy, *J. King Saud Univ., Sci.*, 2022, **34**(4), 102000, DOI: 10.1016/j.jksus.2022.102000.

80 H. Yang, X. Zhang, P. Velu, X. Liu and A. Vijayalakshmi, *Mater. Lett.*, 2022, **313**, 131645, DOI: 10.1016/j.matlet.2021.131645.

81 L. Shabani, S. R. Kasaee, S. Chelliapan, M. Abbasi, H. Khajehzadeh, F. Sadat Dehghani, T. Firuzyar, M. Shafiee, A. M. Amani, S. M. Shirazi, A. Vaez and H. Kamyab, *Appl. Phys. A*, 2023, **129**, 564, DOI: 10.1007/s00339-023-06832-6.